Control of plasma profile in microwave discharges via inverse-problem approach

Yasaka, Yasuyoshi
Tobita, Naoki
Tsuji, Akihiro

(Citation)
AIP Advances,3:122102-122102

(Issue Date)
2013-12

(Resource Type)
journal article

(Version)
Version of Record

(URL)
https://hdl.handle.net/20.500.14094/90002679

AIP Advances

Control of plasma profile in microwave discharges via inverse-problem approach

Yasuyoshi Yasaka, Naoki Tobita, and Akihiro Tsuji

Citation: AIP Advances **3**, 122102 (2013); doi: 10.1063/1.4840735
View online: http://dx.doi.org/10.1063/1.4840735
View Table of Contents: http://scitation.aip.org/content/aip/journal/adva/3/12?ver=pdfcov
Published by the AIP Publishing

AIP ADVANCES **3**, 122102 (2013)

Control of plasma profile in microwave discharges via inverse-problem approach

Yasuyoshi Yasaka,[a] Naoki Tobita,[b] and Akihiro Tsuji[c]
Department of Electrical and Electronic Engineering, Kobe University, Kobe 657-8501, Japan

(Received 13 August 2013; accepted 18 November 2013; published online 9 December 2013)

In the manufacturing process of semiconductors, plasma processing is an essential technology, and the plasma used in the process is required to be of high density, low temperature, large diameter, and high uniformity. This research focuses on the microwave-excited plasma that meets these needs, and the research target is a spatial profile control. Two novel techniques are introduced to control the uniformity; one is a segmented slot antenna that can change radial distribution of the radiated field during operation, and the other is a hyper simulator that can predict microwave power distribution necessary for a desired radial density profile. The control system including these techniques provides a method of controlling radial profiles of the microwave plasma via inverse-problem approach, and is investigated numerically and experimentally. [http://dx.doi.org/10.1063/1.4840735]

I. INTRODUCTION

In plasma-aided manufacturing, plasma uniformity is one of the most important parameters in determining qualities of processing, especially for large wafers. In fabrication lines, a plasma device is given an operating condition from a recipe and generates plasmas and processes wafers with uniformities in variation in radial or azimuthal direction. Several techniques were used to adjust plasma uniformities such as power control,[1–4] gas feed control with multi-nozzle system,[5] pulse power modulation,[6] etc., none of which is sufficient to directly manipulate spatial distribution of plasmas in wide range of parameters.

Furthermore, at present, evaluation and control of the uniformity are performed empirically without the basis of plasma physics. On the other hand, plasma simulation is used to predict 2D or 3D profiles of plasma or radical densities as output for a given input condition, in order to make comparison with experiments, but not to control the device.[7–12] If input and output can be reversed, the simulation code would predict conditions of power and/or gas feed for a desired profile of, for example, plasma density. In the end this may require formulation of a plasma simulation code as inverse problem solver. As a first step, however, one could use forward solvers to construct a code that can virtually obtain a solution of the inverse problem.

We employ two novel techniques to control plasma uniformity in microwave discharges for plasma processing. One is a segmented multi-slot planar (MSP) antenna that can change radial distribution of the radiated field by using two magnetron sources with segmented slot plate. The other is a hyper simulation that can predict microwave power distribution necessary for a desired radial density profile using physical model equations.[13] By using a control system consisting of the hyper simulation and the adjustable antenna, it is expected that one can produce a plasma with the

[a]Author to whom correspondence should be addressed. Electronic mail; yasaka@eedept.kobe-u.ac.jp.
[b]Present address; Kansai Electric Power Co., Osaka, Japan.
[c]Present address; Tokyo Electron Limited, Tsukuba, Japan.

profile close to a specified target density profile or can select a desired edge-to-center density ratio in online. In this paper, we describe background on microwave propagation in a non-uniform plasma and explain usefulness of the MSP antenna in controlling radiation profile of the microwave fields. We then investigate plasma production and evaluate density profiles by using the segmented MSP antenna. A practical method, called the hyper simulation, is proposed, where an inverse problem is virtually solved by using the existing 2D fluid simulation code and additional manipulation. Finally, we adopt the control system to the microwave discharge device to test the basic idea of the hyper simulation.

II. CONTROL OF SLOT-EXCITED MICROWAVE PLASMA

A. Microwave propagation

Schematic diagram of the microwave plasma device is shown in Fig. 1(a), where a slot antenna radiates microwave field at a frequency ω through a glass window to an axially non-uniform plasma. The density n_e along the axis is schematically shown at the right. The electromagnetic field is cutoff at a location where ω equals to plasma frequency ω_{pe}, but at the same time, axial electric field E_z, which is parallel to the density gradient, is strongly peaked there to heat electrons, which is called resonant absorption. The values of E_z along the axis is plotted in Fig. 1(b) with the origin at the interface of a glass plate and the plasma. Since the electric field at the resonance location is very large as seen from Fig. 1(b) and the absorption is strong, the microwave propagates to the plasma almost uni-directionally with little reflection. This indicates that the radial and azimuthal profile of power absorption in the plasma can be changed by antenna radiation profile.

B. Segmented slot antenna and plasma device

We have constructed a microwave plasma device for 300 mm wafers where dynamic control of power absorption profile can be performed by changing power outputs of two microwave sources. The cavity space over the slot plate of the MSP antenna is divided into two radial sections as shown in Fig. 2, and driven by a double coaxial feeder to change the balance of powers of the inner and outer sections, P_{in} and P_{out}. This can modify the radial distribution of the antenna radiation and control the radial profile of power absorption in the plasma.

Figure 3 shows the experimental setup for the plasma production by using this antenna. It consists of two microwave sources, two TE_{10}-mode transmission lines with a directional coupler, a power monitor, and a three-stub tuner for each line, a double coaxial feeder, the segmented MSP antenna, a quartz window, and a plasma chamber.

The microwave at 2.45 GHz excited from the microwave source P_{in} propagates in the TE_{10}-mode rectangular waveguide and in the inner coaxial feeder, is supplied to the inner antenna cavity, and radiated from the inner segment of the MSP antenna. In the same way, the microwave excited from the source P_{out} is radiated from the outer segment of the MSP antenna. In the coaxial feeders, the microwave propagates via the TEM mode. Then, it is transferred to the TM mode in the antenna cavity and is radiated through the slot plate of the MSP antenna. The aim of using the double coaxial feeder and the segmented MSP antenna is to adjust the radial distribution of the radiated microwave fields by controlling the power ratio of the microwave sources P_{in} and P_{out}. If the microwave fields are strongly absorbed via resonant absorption described in Sec. II A, the wave fields propagates one-way, from the antenna to the plasma, and the radial distribution of the microwave fields at the MSP antenna traces itself to the plasma. Ar gas is used to produce the plasmas, and the pressure in the chamber is kept constant. The radial distribution of the plasmas is measured by a Langmuir probe set on a fast scanning system.

C. Profiles of produced plasmas

The device shown in Fig. 3 produces plasmas with electron densities $n_e \sim (2-5)\times 10^{11}\mathrm{cm}^{-3}$ and electron temperatures $T_e \sim$ (1.2–3) eV for Ar gas pressures $p_{Ar} = (15-100)$ mTorr. Figure 4

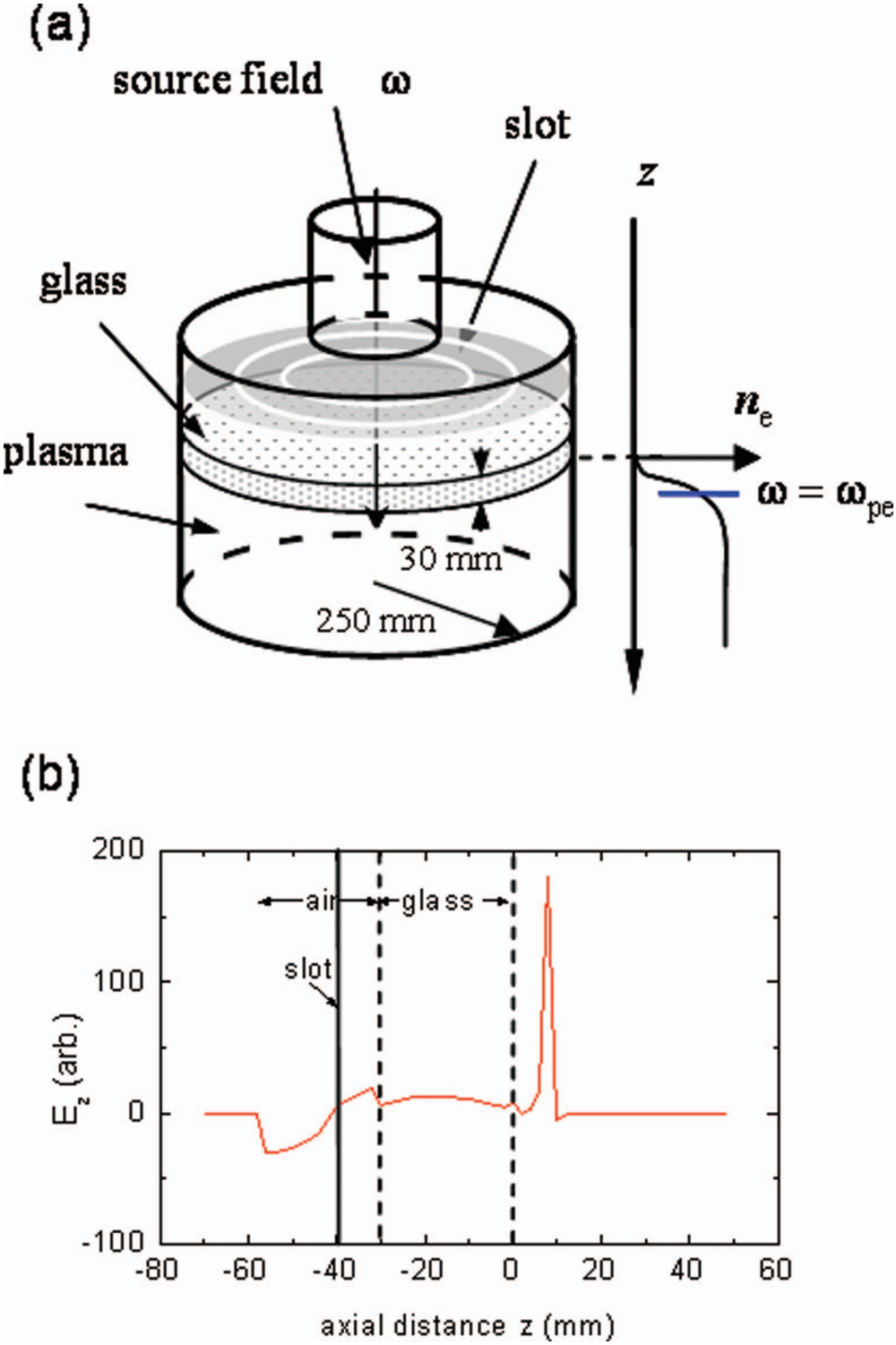

FIG. 1. (a) Sketch of the microwave plasma device and the axial (z) density profile on the right. (b) Plot of E_z along z from the slot, through the air and glass, to the plasma.

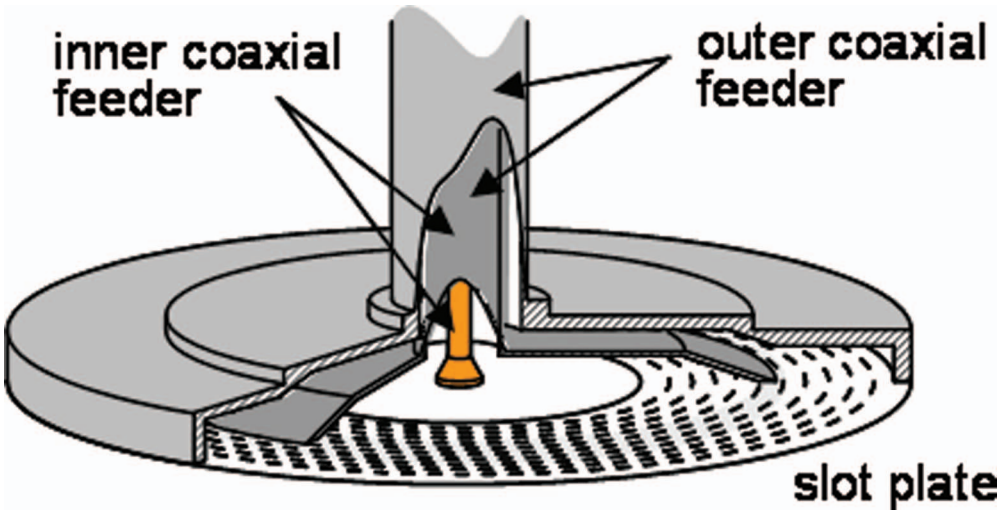

FIG. 2. Segmented MSP antenna with inner and outer coaxial feeders.

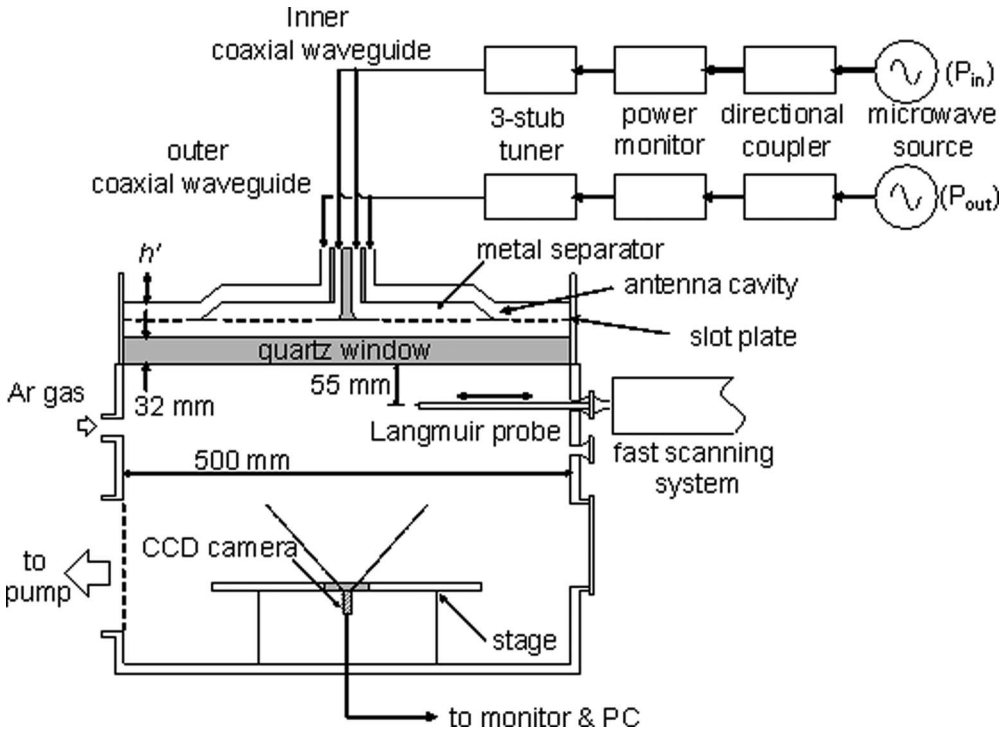

FIG. 3. Setup of the segmented slot antenna and the discharge chamber.

shows the dependence of the radial profile of the ion saturation current density J_{is} on the incident microwave power from the source P_{in}. Here, P_{out} is fixed to 180 W. The other plasma production conditions are $p_{Ar} = 31.0$ mTorr and the flow rate $Q_{Ar} = 66$ sccm. Also, in the graph, parenthetic values for P_{in} represent the reflected power. As shown in Fig. 4, produced plasmas exhibit radially smooth distribution from the center to the radius of 15 cm, corresponding to the size of 8-inch wafer. It shows that J_{is} near the center increases by increasing P_{in}, and J_{is} for $15 \leq r \leq 20$ cm almost remains constant by increasing P_{in}.

Figures 5(a) and 5(b) show the dependence of the plasma uniformity and the gradient of J_{is} in the radial distribution on the power ratio (P_{in} /P_{out}), respectively, where each value is for J_{is} in

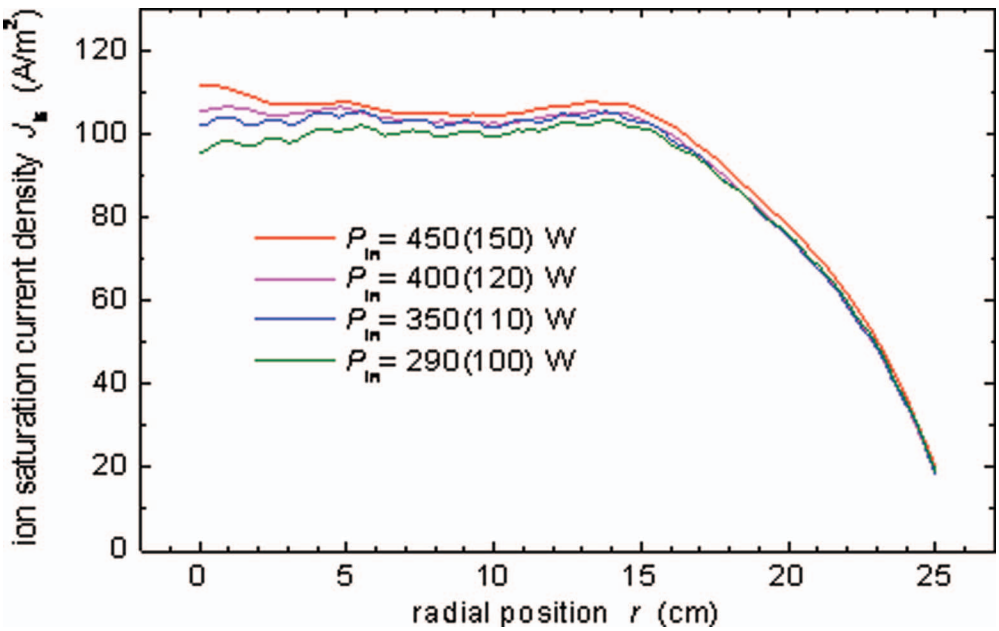

FIG. 4. Radial profiles of the ion saturation current density for several values of P_{in} with a fixed value of $P_{out} = 180$ W.

$r \leq 15$ cm. Here, $p_{Ar} = 31.0$, 47.1, and 80.5 mTorr. The plasma uniformity of J_{is} is calculated by $\sigma(J_{is})$ / [2 × ave(J_{is})] × 100 %, where $\sigma(J_{is})$ and ave(J_{is}) represent the standard deviation, and average values, respectively. The gradient is calculated by [$J_{is}(15) - J_{is}(0)$] / [$J_{is}(15) + J_{is}(0)$] × 100 %, where the numbers associated with J_{is} are the radial position in the unit of cm.

In Fig. 5(a), the radial distribution uniformity is improved by increasing the power ratio, P_{in} /P_{out}, and the plasmas with the best uniformity are produced near P_{in} /$P_{out} \approx 1.0$–1.5 for various p_{Ar}. The uniformity becomes worse when the power ratio is increased further. It shows that the plasmas with good uniformity in the radial distribution can be produced for a wide range of p_{Ar} by using the segmented MSP antenna. In Fig. 5(b), the radial profile of the plasmas changes from upward slant to downward slant, from left to right, by increasing the power ratio. It shows that the radial profile of plasmas can be adjusted in various p_{Ar} by changing the power ratio.

It can be said that the present microwave discharge device with the segmented MSP antenna has a function that the radial profiles can be controlled by the power ratio of the inner to the outer segments.

III. HYPER SIMULATOR

We have shown in the previous section that our microwave discharge device is capable of changing the radial distribution of plasma profiles by controlling the power absorption profile of the plasma, which can be directly adjusted by the power ratio of the two microwave sources connected to inner and outer segments of the MSP antenna. We are developing a system that controls radial distribution of plasmas so that it coincides with a profile given by an operator. Usually, this kind of control is realized by a feedback control system consisting of a plasma monitor, a control software based on empirical methods, and a device manipulator. In our system, the simulator with reversed input and output as compared to general plasma simulation codes, which we call a hyper simulator, is used to obtain device parameters necessary for producing the plasma with the given radial profile. Although the hyper simulator must finally be constructed as an inverse problem solver, we here use a direct problem simulation part combined with a transfer function part iteratively to get a practical solution of the inverse problem.[14] It should also be noted that the plasma monitor in the control system is optional since the hyper simulator reproduces behaviors of the target plasma device.

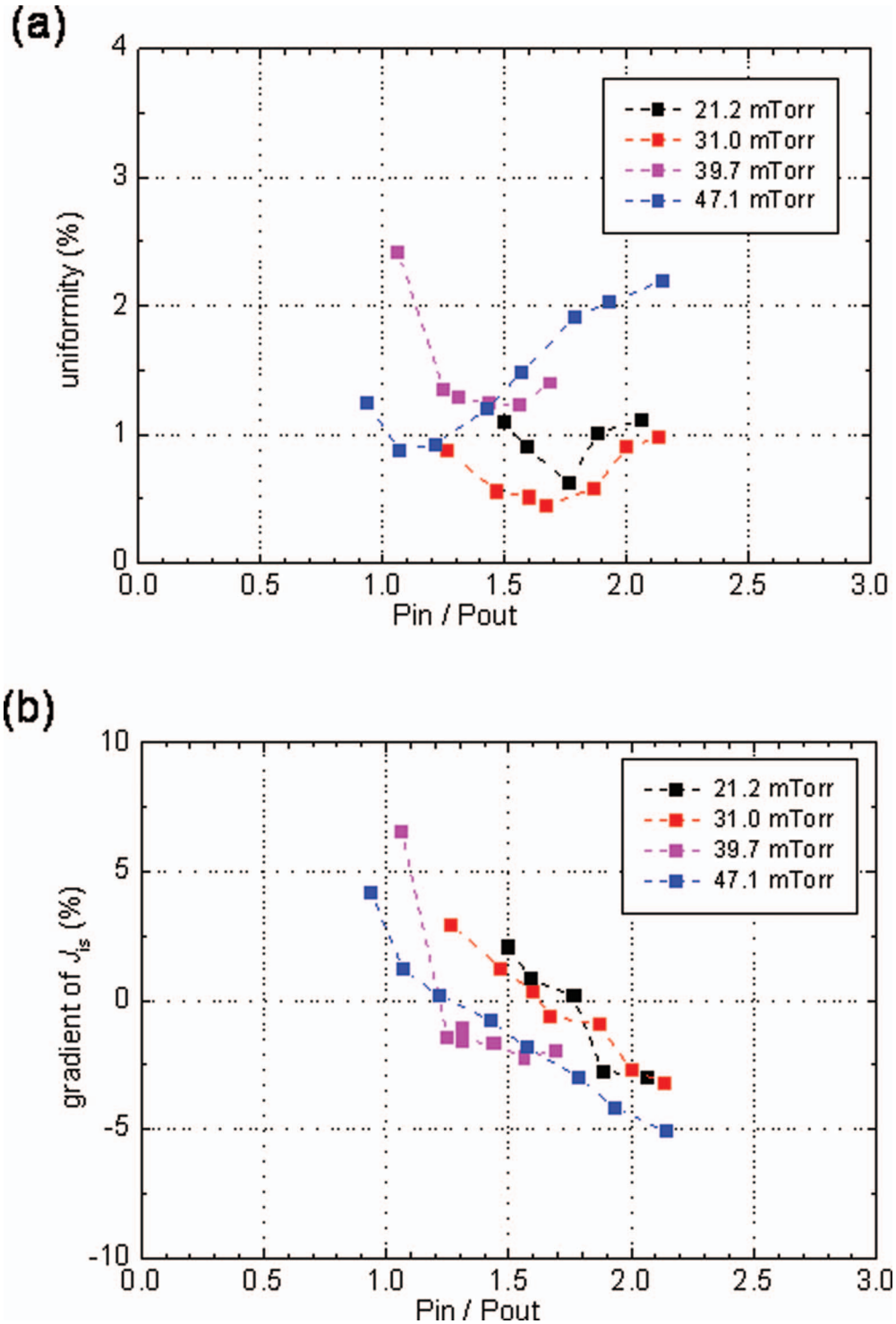

FIG. 5. (a) Plasma uniformity for $r \leq 15$ cm and (b) radial gradient of J_{is} as a function of the power ratio, P_{in} /P_{out} for several values of p_{Ar}.

A. Two dimensional fluid code

In developing a code for the direct problem simulation part, the discharge chamber used in the experiment as shown in Fig. 3 is modeled. The waveguide, air layer, a slot plate, another air layer, quartz glass window, and plasma are layered. The source electric field at frequency of 2.45 GHz is applied at the center of each waveguide. In the model, slots of the antenna are continuous in the azimuthal direction. We employ a standard finite difference time domain (FDTD) scheme or finite element method (FEM) to solve Maxwell equations for the electric field $\boldsymbol{E}$ and the magnetic field $\boldsymbol{B}$;

$$\begin{aligned} \frac{\partial}{\partial t}\boldsymbol{B} &= -\nabla \times \boldsymbol{E}, \\ \frac{\partial}{\partial t}\boldsymbol{E} &= c^2 \nabla \times \boldsymbol{B} - \frac{1}{\varepsilon_0}\boldsymbol{J}, \end{aligned} \tag{1}$$

and the equation of motion of electrons under microwave fields for the current density $\boldsymbol{J}$;

$$\frac{\partial}{\partial t}\boldsymbol{J} = \varepsilon_0 {\omega_{pe}}^2 \boldsymbol{E} - \sum_j \nu_{mj} \boldsymbol{J}, \tag{2}$$

where ε_0 is the permittivity in vacuum, c is the velocity of light, and ν_m is the momentum transfer collision frequency of electrons with neutral species j. The power absorption of electrons from the microwave fields is calculated using

$$P_{abs}(\boldsymbol{r}, t) = \frac{1}{T}\int_{t-T/2}^{t+T/2} \boldsymbol{J} \cdot \boldsymbol{E} dt, \tag{3}$$

where T is the period of the microwave and the integration is over one period. Note that the time variation of P_{abs} is much slower than microwave oscillation, with which $\boldsymbol{J}$, $\boldsymbol{E}$, and $\boldsymbol{B}$ vary, and is of the order of the time variations of $n_e(\boldsymbol{r}, t)$ and the electron temperature $T_e(\boldsymbol{r}, t)$. The time variations of n_e and T_e are governed by the fluid equations represented by

$$\frac{\partial n_e}{\partial t} + \nabla \cdot (n_e \boldsymbol{u}) = \sum_{j,k} n_j \nu_{kj} n_e, \tag{4}$$

$$\begin{aligned} &\frac{\partial}{\partial t}\left(\frac{3}{2} n_e k_B T_e\right) + \nabla \cdot \left(\frac{5}{2} k_B T_e n_e \boldsymbol{u} + \boldsymbol{q}\right) \\ &= P_{abs} - \sum_j \left(\frac{3m}{M_j}\nu_{mj} k_B T_e - \sum_k n_j \nu_{kj} V_{kj}\right) n_e, \end{aligned} \tag{5}$$

where $\boldsymbol{u}$ is the fluid velocity, $\boldsymbol{q}$ is the thermal flux, k_B is the Boltzmann constant, and ν_{kj} and V_{kj} are the cross section and threshold energy of the k-th-type inelastic collision of electrons to the j-th species. Note that, in Eq. (5), k is for ionization or recombination (while negating the term value). ν is a function of T_e and its values are stored in tables in divisions of 0.5 or 1 eV for every type of collisions. The particle flux $n_{e\mathbf{u}}$ consists of drift and diffusion terms, the former of which is determined by the self-consistent slowly varying static electric field. To save computational time in solving Poisson's equation, we use plasma approximation in which the ion density is equal to n_e and $n_{e\mathbf{u}}$ is represented by ambipolar diffusion: $n_{e\mathbf{u}} = -D_a \nabla n_e$ with the diffusion coefficient D_a, which is a function of T_e. We neglect the sheath thickness and assume that the position of the sheath edge is on the chamber wall. On the sheath edge, the parallel particle and heat flux from the plasma normal to the chamber wall are set equal to those determined by the Bohm sheath criterion. Because the time scale of Eqs. (4) and (5) is much longer than that of eqs. (1) to (3), both sets of equations can be calculated separately.

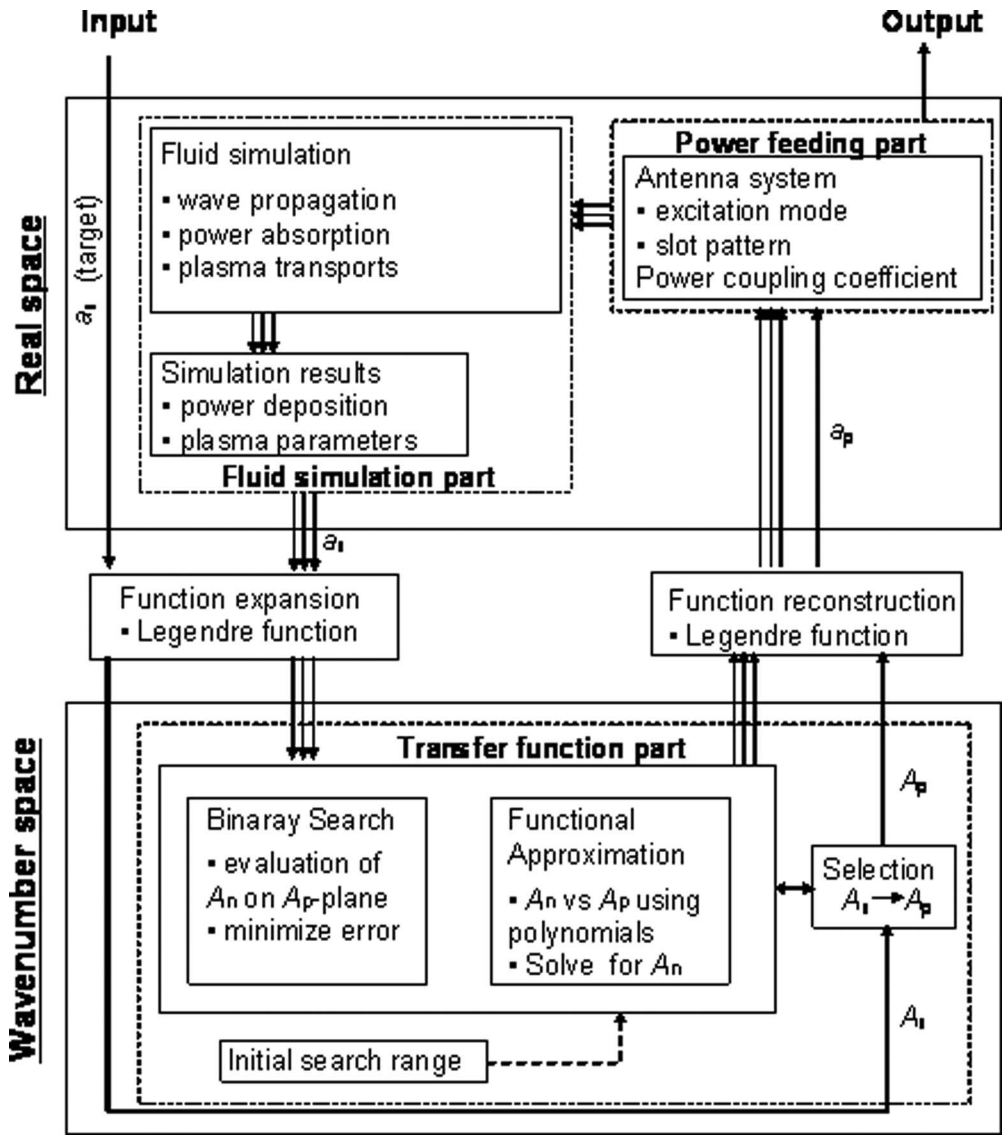

FIG. 6. Diagram of a hyper simulation system.

B. Method for prediction

Figure 6 shows a calculation procedure of the hyper simulator for profile control of the microwave plasma. This simulator has two aims. One is to give the information of the device setting necessary for producing the plasmas with the profile that users hope to create. The other is to add adjusting capability for differences between the experiment and simulation results. The hyper simulator code has the density profile as input and the power absorption profile as output, and is roughly classified into three parts; a power feeding part, a fluid simulation part and a transfer function part.

The power feeding part determines the excitation method, the slot geometry, and the power coupling coefficient a_P given by

$$P_{abs}(r, z) = a_P(r) P_{abs0}(r, z), \tag{6}$$

where P_{abs0} and P_{abs} represent the present power absorption distribution and the modified power absorption distribution, respectively. a_P is a parameter to revise a power absorption distribution in the radial direction.

In the fluid simulation part, a two-dimensional fluid simulation code is used to calculate distribution of the plasma parameters in the steady state as described in the previous section. The relative distribution of $n_e(r, z_0)$ is defined as an $a_N(r)$, where z_0 represents an arbitrary z-directional position for the monitoring. Both the values $a_P(r)$ and $a_N(r)$ are represented by functional expansion as

$$a_S(x) = \sum_n A_S(n) P_n(x) \quad S = P \text{ or } N, \tag{7}$$

where $A_S(n)$ is the spectral intensity of the series of Legendre functions P_n. To use the function expansion for $-1 \le x \le 1, r = R|x|$ is defined assuming the axial symmetry, where R represents the analysis radius. In this case, $A_S(n)$ has only even-order components. Our fundamental investigations find that almost all distributions used in this study can be represented by three low-order components ($n = 0, 2, 4$).

The transfer function part relates $A_N(n)$ and $A_P(n)$, i.e., to find $A_P(n)$ that produces the plasma with a radial distribution represented by $A_N(n)$. At present, two methods are prepared for this purpose. In the binary search method, for the case of $n = 2$ and 4 with normalization; $A_P(0) = 1$, the $A_P(2) - A_P(4)$ space is divided into 3×3 meshes, and the fluid simulation is run with an input of $A_P(n)$ corresponding to a particular mesh point.

The difference in $A_N(n)$ of the calculated profile of the plasma density from the target profile is calculated at each mesh point, and one quadrant out of 4 is chosen with a criterion that the average of the differences at 4 vertexes of the quadrant is minimum. Then, the chosen quadrant is divided into 3×3 and the procedure is repeated until the difference is sufficiently small.

In functional approximation method, a few tens of run of the fluid simulation are performed with various values of $A_P(2) - A_P(4)$, and each result with $A_N(2) - A_N(4)$ is stored. We can approximate that

$$\begin{aligned} A_N(2) &= [\alpha_2 A_P(2) + \beta_2 A_P(4)]^3, \\ A_N(4) &= [\alpha_4 A_P(2) + \beta_4 A_P(4)]^3, \end{aligned} \tag{8}$$

and numerical coefficients are determined from the stored dataset. By using Newton-Raphson method,[15] we can inversely obtain the values of $A_P(n)$ to realize $A_N(n)$ of the target profile from the following equation;

$$\begin{pmatrix} A_P(2) \\ A_P(4) \end{pmatrix}_{m+1} = \begin{pmatrix} A_P(2) \\ A_P(4) \end{pmatrix}_m - J^{-1} \left\{ \begin{pmatrix} A_N(2) \\ A_N(4) \end{pmatrix}_m - \begin{pmatrix} A_N(2) \\ A_N(4) \end{pmatrix}_{\text{target}} \right\}, \tag{9}$$

where m is the iteration number and J is the Jacobian matrix, the elements of which are represented by the numerical coefficients in Eq. (8) and m-th $A_P(n)$. The iteration in Eq. (9) is repeated until conversion is obtained.

The hyper simulator in Fig. 6 calculates $a_P(r)$ necessary to produce the plasma with $a_N(r)$ that is given as the target profile, as an indirect inverse problem solver. The calculation result of $A_P(n)$ is transformed into the parameters of the device manipulation and modification of the operation condition of the device is performed.

IV. RESULTS OF PROFILE CONTROL

A. Conventional fluid simulation

The analyzed device consists of the double coaxial waveguide of WX-39D and -20D type, two cavity spaces, the segmented slot plate, a quartz window and a plasma chamber as shown in Fig. 3. The microwave driven at $\omega/2\pi = 2.45$ GHz propagates via the waveguide and is radiated to the plasma from the slot. We perform a conventional 2-D simulation (the fluid simulation part in Fig. 6) using equations given in Sec. III A with the input of a given power values of P_{in} and P_{out}, and

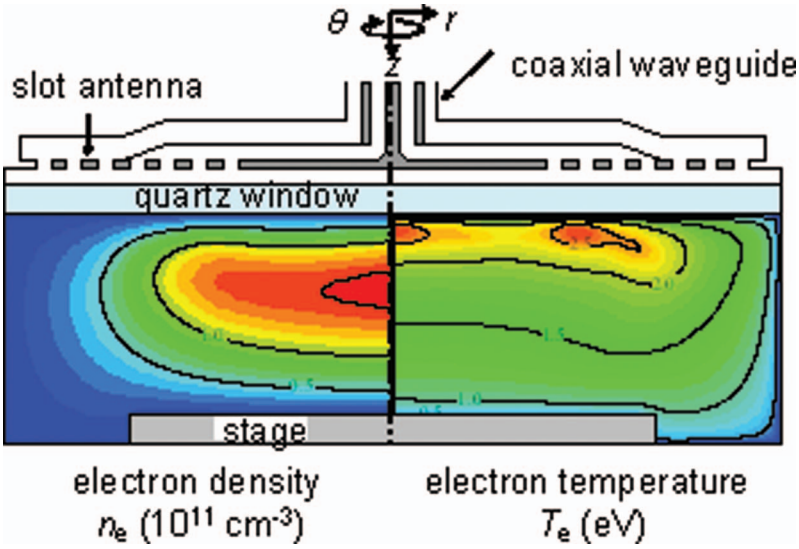

FIG. 7. Simulation result of $n_e(r, z)$ (left half) and $T_e(r, z)$ (right half) for the case of $a_P(r) = 1$ with $P_{\text{in}} / P_{\text{out}} = 1.17$.

no midification of the power absorption profile; $a_P(r) = 1$. In this simulation, the plasma chamber is uniformly filled with Ar gas.

Figure 7 shows the simulation result of $n_e(r, z)$ (left half) and $T_e(r, z)$ (right half) for $p_{\text{Ar}} = 50$ mTorr, the power ratio of $P_{\text{in}} / P_{\text{out}} = 1.17$, and the total incident power of 300 W. The two power sources (actually current segments) are excited in phase, and the simulation time is 3 ms. The radius of the chamber is 25 cm and the depth is 15 cm. The values of n_e and T_e are 1.0−1.4 $\times 10^{11}$ cm^{-3} and 1.5–2 eV around $z = 5$ cm from the bottom of the quartz window. These values are consistent with the experimental results.

The value of $P_{abs}(r, z)$ is known as the simulation output, and we set this result as the reference data, namely,

$$P_{abs}(r, z) = P_{abs0}(r, z), \quad a_P(r) = 1,$$

with the observation position of $z = 5$ cm. In this case, we have $A_P(0) = 1$, $A_P(2) = 0$, $A_P(4) = 0$.

Values of $A_P(2)$ and $A_P(4)$ obtained from the calculated $P_{abs}(r, z)$ and $P_{abs0}(r, z)$ are plotted in Fig. 8 for several values of $P_{\text{in}} / P_{\text{out}}$. This graph inversely gives the value of $P_{\text{in}} / P_{\text{out}}$ necessary to set $P_{abs}(r, z)$ characterized by $A_P(2)$ and $A_P(4)$ with $a_P(r) = 1$.

Next, we set $a_P(r)$ other than 1 to modify the power absorption profile with the other conditions are fixed. The parameters chosen are $A_P(0) = 1$, $A_P(2) = 0.25$, $A_P(4) = -0.375$.

The profiles of $n_e(r, z)$ (left half) and $T_e(r, z)$ (right half) are plotted in Fig. 9 for $a_P(r)$ determined by these parameters with the other conditions being the same as in Fig. 7. We see that the profile of $n_e(r, z)$ changes much so that the center peak observed in Fig. 7 is disappearing and the profile is more flat over the radial direction.

B. Hyper simulator and profile control

Our strategy to control the radial density profile (or J_{is} profile) is as follows;

1. Set a target density profile by values of $A_N(n)$
2. Set the condition of the hyper simulation such as the geometry, p_{Ar}, initial $P_{\text{in}} / P_{\text{out}}$, etc. and $A_N(n)$
3. Run the hyper simulator with the binary search or the functional approximation method to find $A_P(n)$ that produces the target $A_N(n)$
4. Get the value of $P_{\text{in}} / P_{\text{out}}$ for calculated $A_P(n)$ using Fig. 8
5. Set the experimental condition to the value of $P_{\text{in}} / P_{\text{out}}$, and obtain the target profile

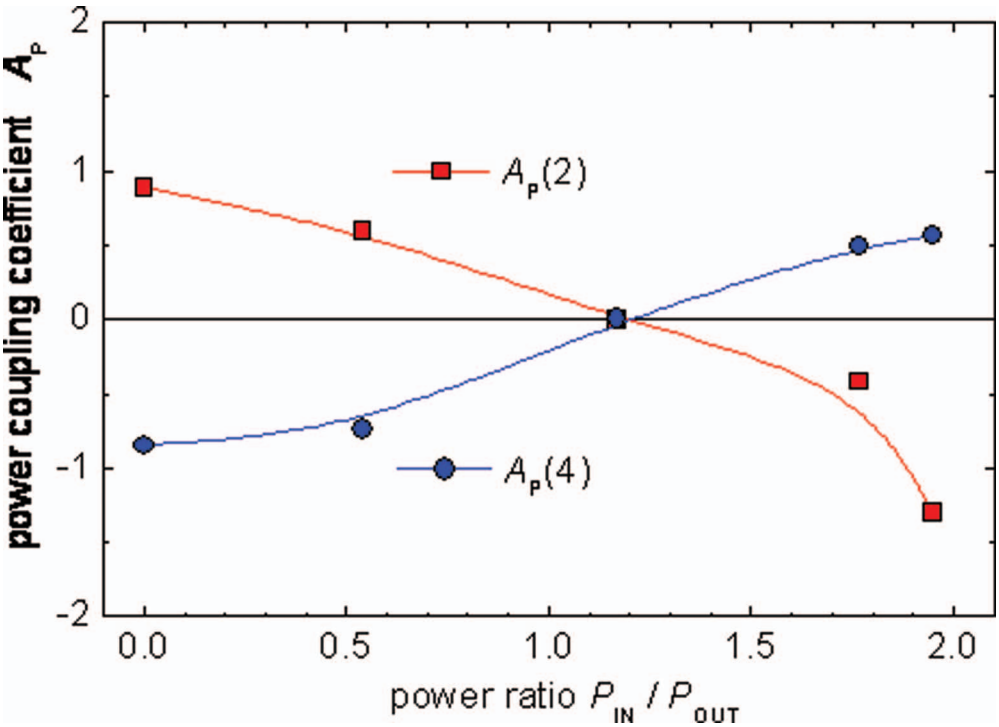

FIG. 8. Values of $A_P(2)$ and $A_P(4)$ obtained from the calculated $P_{abs}(r, z)$ and $P_{abs0}(r, z)$ given in Fig. 7 for several values of P_{in} / P_{out}.

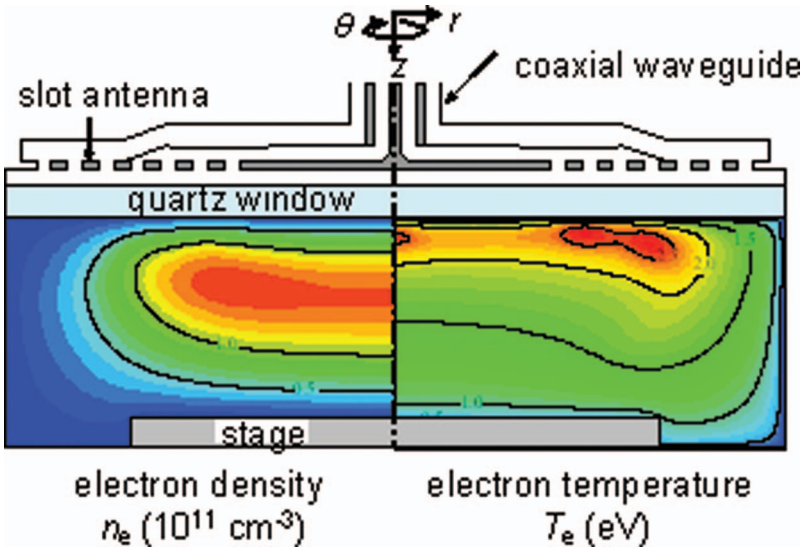

FIG. 9. Simulation result of $n_e(r, z)$ (left half) and $T_e(r, z)$ (right half) for the case of $A_P(0) = 1$, $A_P(2) = 0.25$, $A_P(4) = -0.375$ with P_{in} / $P_{out} = 1.17$.

In Fig. 10, a target density profile is given by open circles as a relative value of $a_N(r)$. This curve is represented by $A_N(n)$, which is to be sent to the hyper simulator. Here, we set the analysis radius $R = 20$ cm used in Eq. (7). The hyper simulator code calculates necessary condition of $A_P(n)$ as well as the density profile for that condition. The solid line in Fig. 10 represents the density profile

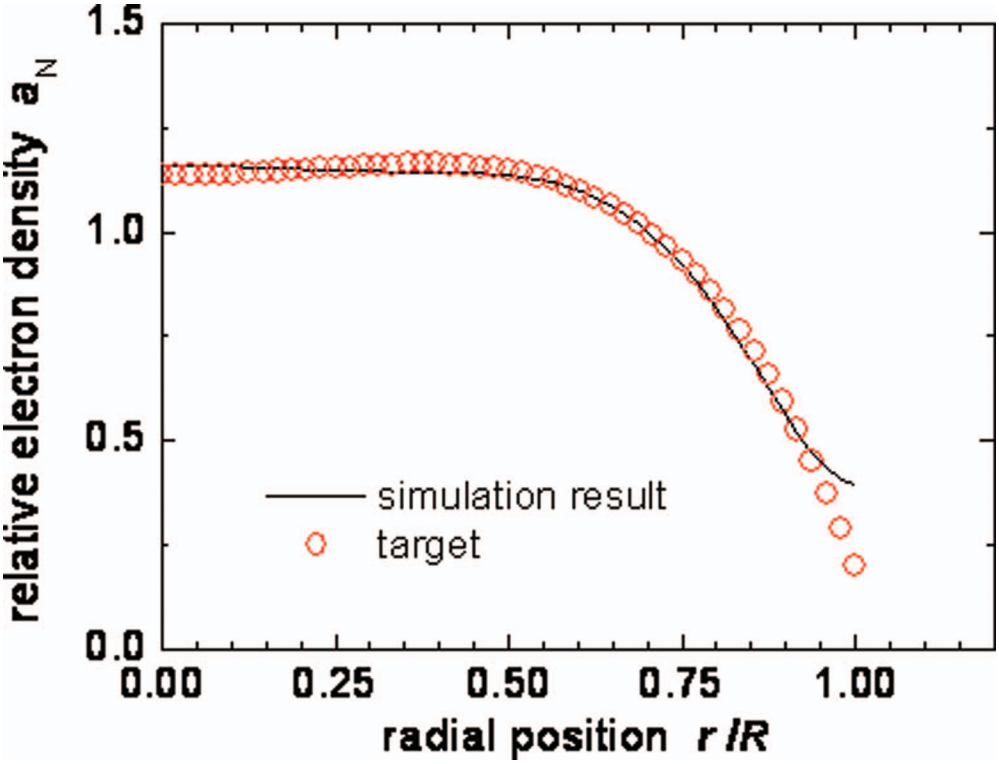

FIG. 10. A target radial density profile (open circles) and the simulator output (solid line).

at an optimal condition of $A_P(0) = 1$, $A_P(2) = 0.25$, $A_P(4) = -0.50$. The target and the calculated profiles are very close indicating that the hyper simulation predicts appropriate condition.

Figure 11(a) is the similar plot as Fig. 10 with the target density profile (open circles) that has a hollow shape or the positive gradient (See Sec. II C).

The hyper simulator has produced the output of $A_P(2) = 0.50$, $A_P(4) = -0.50$ modifing the reference case of $P_{in} / P_{out} = 1.17$, the total power of 300 W, and $p_{Ar} = 50$ mTorr, with the predicted density profile plotted by the solid line in Fig. 11(a). We now set the experimental condition according to this output of the hyper simulator. For the values of $A_P(n)$ described above, we note from Fig. 8 that the value of P_{in} / P_{out} should be 0.52. The experimental device is operated with the close condition of $p_{Ar} = 49.6$ mTorr and $P_{in} / P_{out} = 0.5$ to obtain the measured J_{is} profile plotted in Fig. 11(b). In a practical system in near future, of course, these procedures are to be performed automatically. The experimental profile of the plasma in Fig. 11(b) has the similar characteristics as in (a) in the sense that both profiles have hollow shape and peak at outer radii. One of the differences is that the positions of the outer peak do not coincide.

Figure 12 shows the results as in Fig. 11 for the case of the target profile that is peaked at the center.

In this case, the predicted values from the hyper simulation are $A_P(2) = -1.30$, $A_P(4) = 0.56$, suggesting P_{in} / P_{out} to be around 2.0. The same setting in the experiment gives the measured J_{is} profile plotted in Fig. 12(b). We again find an overall agreement with the target profile and the experimental profile. The discrepancy of the positions of "shoulder" in the profiles are noticeable.

Finally, we set the target profile in between the cases of Fig. 11 and Fig. 12, i.e., mostly flat over the radius of $\sim$ 15 cm. The same plots are given in Fig. 13. The resultant experimental profile corresponds to the simulator output.

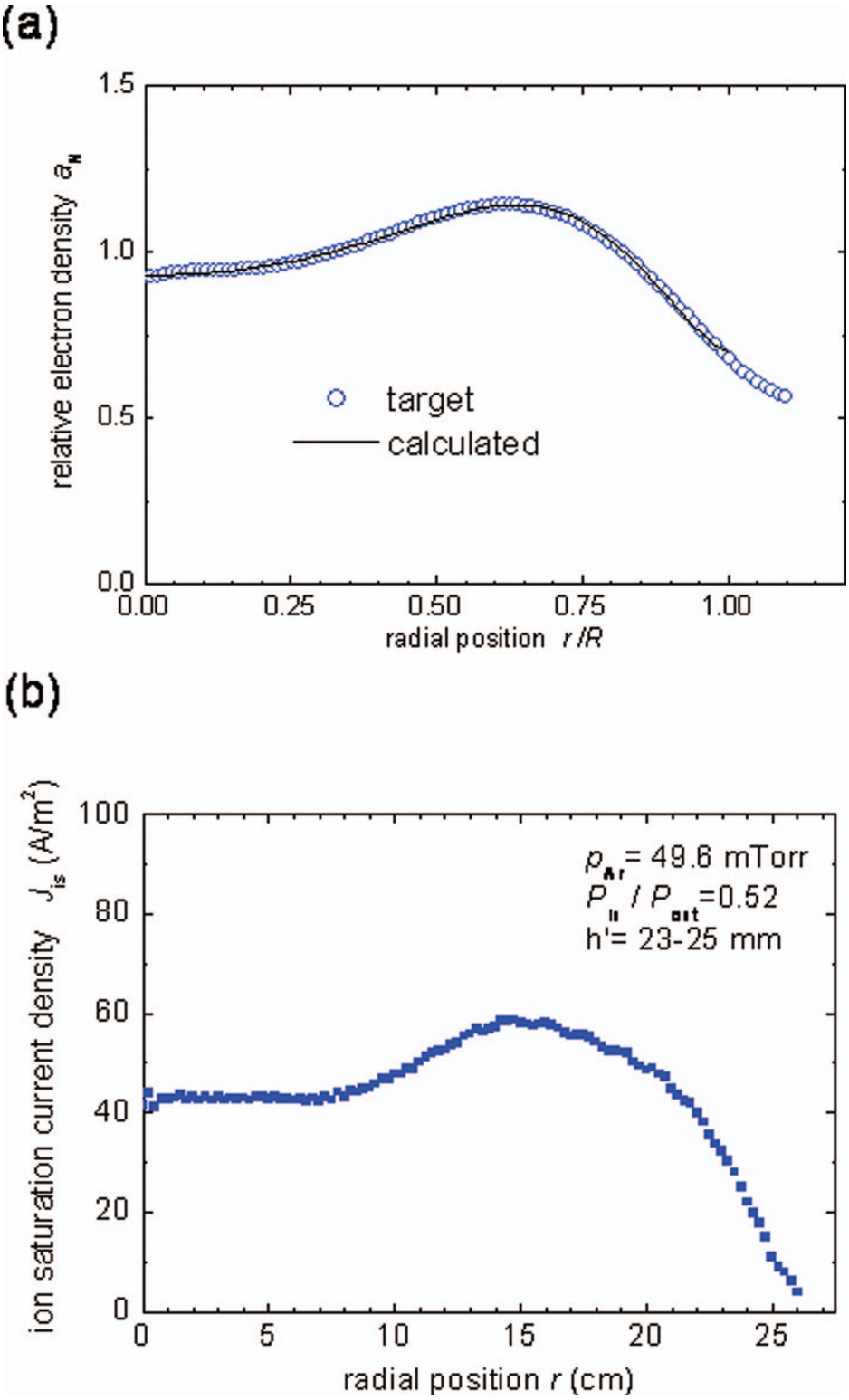

FIG. 11. (a) A target radial density profile (open circles) and the simulator output (solid line), (b) Experimentally observed J_{is} profile when the value of P_{in} / P_{out} is set according to the hyper simulation.

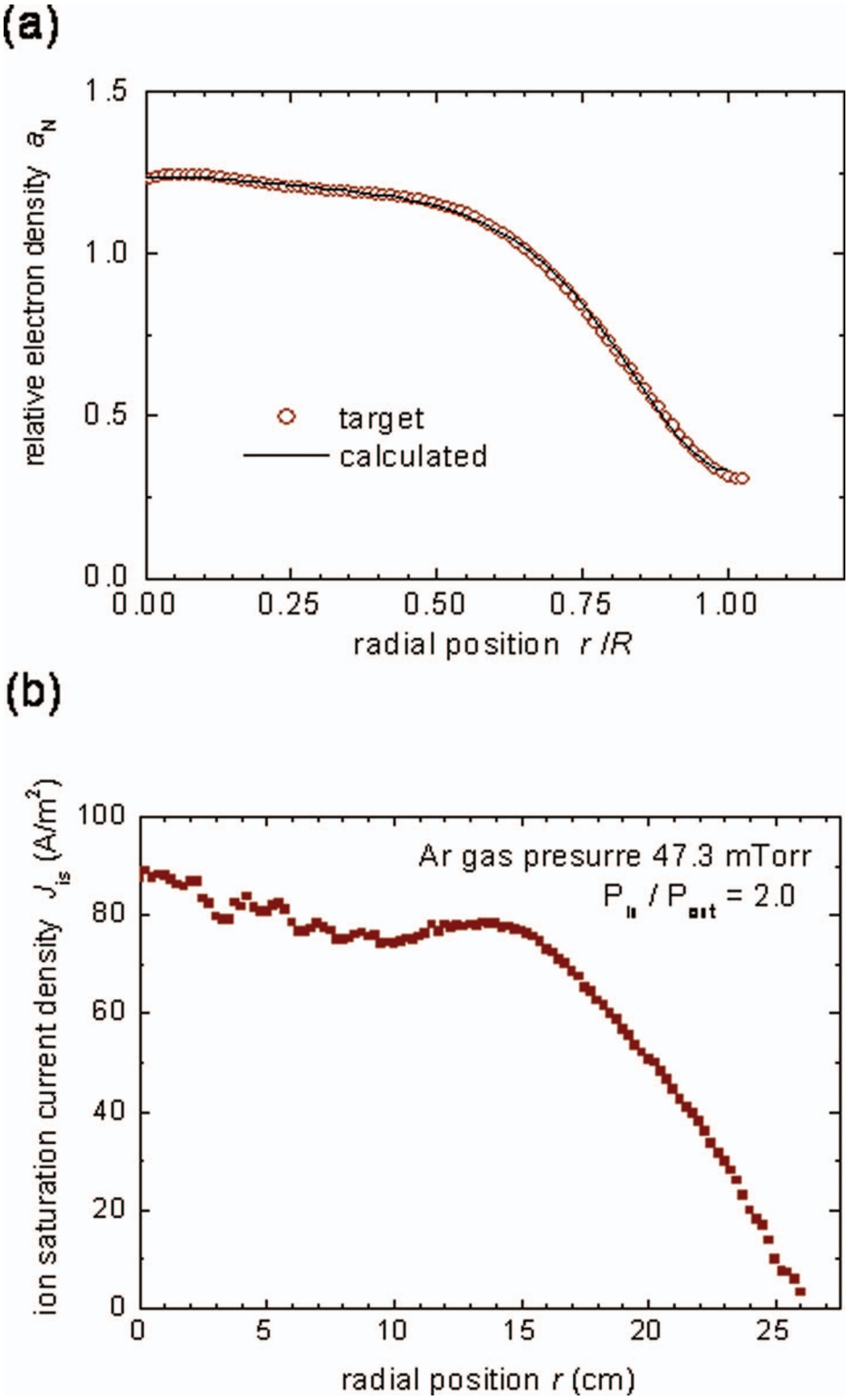

FIG. 12. (a) A target radial density profile (open circles) and the simulator output (solid line), (b) Experimentally observed J_{is} profile when the value of P_{in} / P_{out} is set according to the hyper simulation.

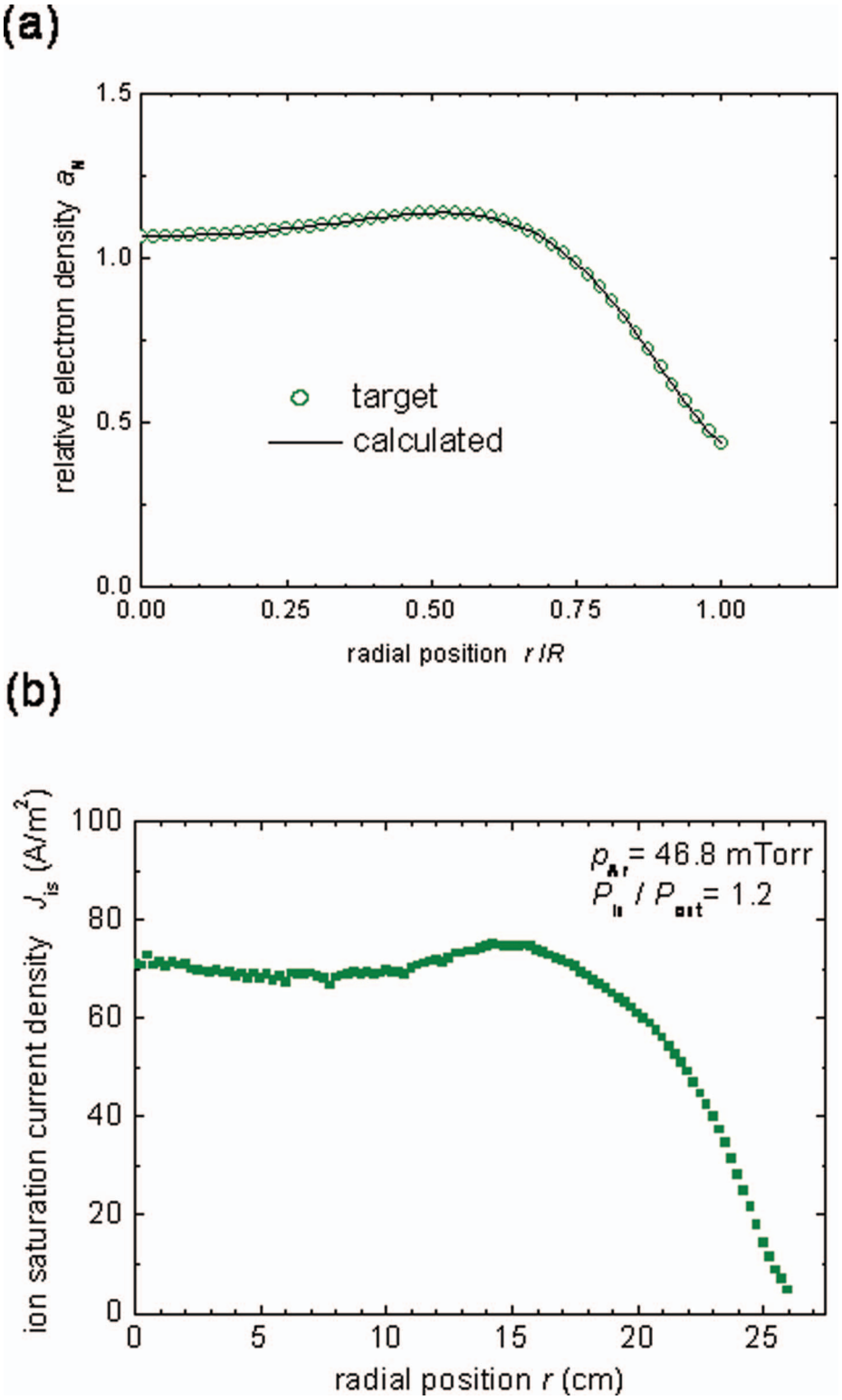

FIG. 13. (a) A target radial density profile (open circles) and the simulator output (solid line), (b) Experimentally observed J_{is} profile when the value of P_{in} / P_{out} is set according to the hyper simulation.

V. SUMMARY

We have presented two novel techniques to control the radial density profiles of microwave discharges; one is the segmented slot antenna that can change distribution of the radiated power in real time during operation, and the other is the hyper simulator that can predict microwave power distribution necessary for a desired radial density profile using physical model equations. Descriptions of both techniques include the experimental results demonstrating profile control by the segmented slot antenna and the detailed procedure and method of the hyper simulator. The control system consisting of the hyper simulator and the segmented slot antenna to obtain a target density profile is demonstrated to work in particular set of conditions. Improved accuracy of the control and on-line manipulation will be added in future.

ACKNOWLEDGMENTS

The authors thank Dr. A. Tsuji for his help in experiments and simulation. This work was supported in part by a Grant-in-Aid for Scientific Research (B) (23340178) from the Japan Society for the Promotion of Science.

[1] K. Bera, S. Rauf, A. Balalkrishna, and K. Collins, IEEE Trans. Plasma Sci. **38**, 3241 (2010).
[2] H-J. Lee, H-C. Lee, Y-C. Kim, and C-W. Chung, Plasma Sources Sci. Technol. **22**, 032002(5pp) (2013).
[3] K. Takenaka, Y. Setsuhara, K. Nishisaka, and A. Ebe, Plasma Process. Polym. **6**, S278 (2009).
[4] S. Shannon, US Patent Application Publication, "Method and System for Controlling Center-to-Edge Distribution of Species within a Plasma," US 2009/0218315 A1 (2009).
[5] S. Banna, A. Agarwal, K. Tokashiki, *et al.*, IEEE Trans. Plasma Sci. **37**, 1730 (2009).
[6] Y. Yasaka, K. Koga, N. Ishii, T. Yamamoto, M. Ando, and M. Takahashi, Phys. Plasmas **9**, 1029 (2002).
[7] D. Economou, Thin Solid Films **365**, 348 (2000) and references therein.
[8] M. Kushner, J. Phys. D: Appl. Phys. **42**, 194013(20pp) (2009).
[9] R. Kinder and M. Kushner, J. Vac. Sci. Technol. **A19**, 76 (2001).
[10] T. Morimoto, Y. Yasaka, M. Tozawa, T. Akahori, H. Amano, and N. Ishii, Jpn. J. Appl. Phys. **36**, 4769 (1997).
[11] A. Tsuji, Y. Yasaka, S.-Y. Kang, T. Morimoto, and I. Sawada, Thin Solid Films **516**, 4368 (2008).
[12] Y. Yasaka, A. Sakae, N. Sugimoto, H. Takeno, and H. Hojo, Jpn. J. Appl. Phys. **45**, 8059 (2006).
[13] Y. Yasaka and A. Tsuji, Bul. APS, 52nd Ann. Mtg., Div. Plasma Phys., Chicago, **JO7-10**, 161 (2010).
[14] A. Tsuji and Y. Yasaka, Jpn. J. Appl. Phys. **50**, 08JC03 (2011).
[15] W. H. Press, S. A. Teukolsky, W. T. Vetterling, and B. P. Flannery, *Numerical Recipes* (Cambridge University Press, New York, 2007) 3rd ed., p. 456.